# Unsupervised Feature Selection Algorithm Based on $L_{2,p}$-norm Feature Reconstruction

Wei Liu [1,☯,*], Qian Ning[1,☯], Guangwei Liu[2], Haonan Wang[3], Yixin Zhu[1], Miao Zhong[1]

**1** College of Science, Liaoning Technical University, Fuxin, Liaoning, China,
**2** College of Mines, Liaoning Technical University, Fuxin, Liaoning, China,
**3** Johns Hopkins University, Maryland, USA

☯These authors contributed equally to this work.
* liuwei@lntu.edu.cn

## Abstract

Traditional subspace feature selection methods typically rely on a fixed distance to compute residuals between the original and feature reconstruction spaces. However, this approach struggles to adapt to diverse datasets and often fails to handle noise and outliers effectively. In this paper, we propose an unsupervised feature selection method named unsupervised feature selection algorithm based on $l_{2,p}$-norm feature reconstruction (NFRFS). Employing a flexible norm to represent both the original space and the spatial distance of feature reconstruction, enhances adaptability and broadens its applicability by adjusting $p$. Additionally, adaptive graph learning is integrated into the feature selection process to preserve the local geometric structure of the data. Features exhibiting sparsity and low redundancy are selected through the regularization constraint of the inner product in the feature selection matrix. To demonstrate the effectiveness of the method, numerical studies were conducted on 14 microarray benchmark datasets. Our results indicate that the method outperforms 10 unsupervised feature selection algorithms in terms of clustering results.

## 1. Introduction

In this field of information explosion, traditional data processing methods are facing unprecedented challenges due to the vast amount of data and the high dimensionality. The efficient and accurate processing of these rapidly growing high-dimensional datasets and extracting key information has become a focal point of attention and research in fields such as data mining [1], pattern recognition [2], and machine learning [3]. Feature selection algorithms extract representative features from raw data, not only achieving dimensionality reduction but also preserving the physical significance of the data [4].

Based on whether the data includes label information, feature selection can be divided into three types: supervised, semi-supervised, and unsupervised [5]. Since unsupervised feature selection does not rely on label information, it identifies features that best represent the characteristics of the data by analyzing its intrinsic structure, making it of significant research importance and value [6]. According to evaluation criteria, feature selection methods can be classified into filter, wrapper, and embedded methods [7]. Embedded methods combine the advantages of both filter and wrapper methods, integrating the feature selection process into model training to enhance the performance of algorithms [8].

Graph structure is crucial for feature selection. Authors in [9] introduced the Laplacian Score algorithm, which is based on the relationships between data points. This algorithm evaluates the importance of each feature by calculating its Laplacian score, reflecting its ability to preserve local information. A study in [10] introduced a feature selection algorithm based on latent representation learning and manifold regularization. By combining latent representation learning using non-negative matrix factorization and graph-based manifold regularization, it performs feature selection in a robust latent space, capturing the intrinsic structure of the data and reducing the negative impact of noise. This approach, which relies on a fixed similarity graph and depends on the sample similarity matrix, separates the construction of the graph from the learning of the feature selection matrix. Therefore, it is susceptible to the influence of noise or outliers. Therefore, literature [11] proposed an unsupervised feature selection algorithm based on adaptive structure learning, which simultaneously conducts feature selection and data structure learning to better capture both global and local structures of the data. In literature [12], the unsupervised feature selection method known as Self-Weighted Adaptive Graph-based Minimum-Redundant Subspace Learning is mentioned. This approach integrates adaptive self-weighted graph learning, minimum redundancy, and sparsity constraints into a comprehensive framework. Manifold regularization can preserve the inherent geometric structure of the data, so unsupervised feature selection algorithms that incorporate manifold regularization typically achieve better performance. Although these algorithms have made some improvements, they need to enhance their handling of redundant information during feature selection.

In recent years, regularizers are often used to constrain the feature selection matrix in dealing with redundant information [13]. A study in [14] combined spectral analysis with $l_1$-norm regularization and proposed the multi-cluster feature selection algorithm. Authors in [15] unified feature selection and similarity matrix construction into a single framework and used an $l_{2,0}$-norm constraint on the feature selection matrix to achieve feature selection. In Reference [16], the authors introduced non-negative constraints and applied an $l_{2,p}$-norm to the matrix of feature transformations. This approach, in comparison to the $l_{2,1}$-norm, offers a more tractable optimization process. The variable $p$ allows for a flexible trade-off between row sparsity and the convexity of the model, potentially enhancing the model performance. Meanwhile, Reference [17] incorporated the absolute values of inner product outcomes between the vectors of the feature selection matrix as a regularization component, thus fully accounting for feature interdependencies in the pursuit of a more independent selection of the subset of features. Influenced by the norms used in the feature selection matrix, regularizers can also be added to the loss function to prevent model overfitting and promote sparsity. Common choices include $F$-norm and $l_{2,1}$-norm, but both assume a fixed distance between the original samples and predicted labels, which limits their ability to flexibly adjust this distance based on the data's structure. Therefore, Reference [18] proposed a feature selection method based on the $l_{2,p}$-norm and sample constraints, applied in the diagnosis of Alzheimer's disease.

Motivated by these considerations, we propose an efficient technique for feature selection, called an unsupervised feature selection algorithm based on $l_{2,p}$-norm feature reconstruction (NFRFS). The distance between the original space and the reconstructed subspace can be flexibly adjusted through the $l_{2,p}$-norm. In this approach, graph embedding and feature selection interact to learn local structural information between data points. Inner product regularization is employed to select features that are both low in redundancy and sparse. The effectiveness of this method has been demonstrated on 12 benchmark datasets.

The main contributions of this paper are as follows:

- In the reconstruction error, a more flexible $l_{2,p}$-norm is used to measure the

distance between the original samples and the reconstructed samples, and the value of $p$ is adjusted to handle noise and outliers in the dataset.

- The feature selection matrix is sparsified by utilizing the inner product sparse regularization, selecting representative features with low redundancy.
- Comprehensive experiments on 14 benchmark datasets show that NFRFS is superior to several state-of-the-art feature selection methods. The experimental results validate the effectiveness and practicality of the model.

The rest of the paper is organized as follows. Section 2 explains some basic notions and definitions. In Section 3, we propose an optimization problem for feature selection and an iterative algorithm for solving the problem. In Section 4, various experimental results are analyzed. Conclusions are drawn in Section 5.

# 2. Related work

## 2.1. Notation and definition

To help explain the details of the proposed algorithm, some notations need to be introduced in advance. For a matrix $X \in \mathbb{R}^{n\times d}$ , its $l_{r,s}$-norm can be defined as follows:

$$\|X\|_{r,s} = \left(\sum_{i=1}^{d}\left(\sum_{j=1}^{n} x_{ij}^{r}\right)^{\frac{s}{r}}\right)^{\frac{1}{s}}$$

The norm is called the $F$-norm or the $l_2$-norm when $r = s = 2$. Based on the above definition of the norm, the $F$-norm and $l_{2,p}$-norm of matrix are calculated as

$$\|X\|_F = \left(\sum_{i=1}^{d}\sum_{j=1}^{n} x_{ij}^{2}\right)^{\frac{1}{2}}$$

$$\|X\|_{2,p} = \left(\sum_{i=1}^{d}\left(\sum_{j=1}^{n} x_{ij}^{2}\right)^{\frac{p}{2}}\right)^{\frac{1}{p}}$$

More details are listed in table 1.

**Table 1. The notations used in this paper.**

| Notation | Description |
|---|---|
| $n$ | Number of samples |
| $d$ | Original spatial dimension |
| $l$ | The number of selected features |
| $x^i$ | The $i$-th row of $X$ |
| $x_j$ | The $j$-th column of $X$ |
| $x_{ij}$ | The element in $i$-th row and $j$-th column of $X$ |
| $s_{ij}$ | The similarity between the sample points $x_i$ and $x_j$ |
| $X \in \mathbb{R}^{n\times d}$ | Original data matrix |
| $W \in \mathbb{R}^{d\times l}$ | The feature selection matrix |
| $H \in \mathbb{R}^{l\times d}$ | The reconstruction coefficient matrix |
| $I \in \mathbb{R}^{l\times l}$ | The identity matrix |
| $L \in \mathbb{R}^{n\times n}$ | The Laplacian matrix |
| $S \in \mathbb{R}^{n\times n}$ | The similarity matrix of data space |
| $D \in \mathbb{R}^{n\times n}$ | Diagonal matrix |
| $X^T$ | The transpose of $X$ |
| $tr(X)$ | The trace of $X$ |
| $\langle a, b\rangle$ | The inner product of $a$ and $b$ |

## 2.2. Feature Reconstruction in Subspace Using $l_{2,p}$-norm

Facing the challenges of high dimensionality and excessive redundant information, Wang [19] proposed an algorithm from the perspective of subspace learning. The algorithm extracts a low-dimensional subspace from high-dimensional data, which can represent the main information of the original feature space while removing redundancy and noise.

$$\begin{aligned} &argmin\, \|X - XWH\|_F^2 \\ &s.t. W.H \geq 0, W^T W = I_l \end{aligned} \tag{1}$$

Where $H \in \mathbb{R}^{l\times d}$ is the coefficient matrix used for reconstruction, which maps the learned subspace to the original space. $l$ represents the number of selected features, and $I \in \mathbb{R}^{l\times l}$ is an identity matrix. $W \in \mathbb{R}^{d\times l}$ is the feature selection matrix, constrained with orthogonality $W$ to ensure that there is at most one non-zero value per row and column. Additionally, non-negative constraints are imposed on $W$ to preserve its real-world physical meaning [20].

In existing subspace feature selection methods, the $F$-norm is typically used to measure the distance between the original data space and the reconstructed subspace [21]. However, for some datasets, using a fixed distance metric does not result in the optimal feature subset. Therefore, this paper uses an adaptive distance metric to effectively improve model performance, choosing the $l_{2,p}$-norm to constrain the distance between the original space and the reconstructed subspace. The $l_{2,p}$-norm allows for flexible adjustment of the size of parameter $p$, choosing the $p$ parameter most favorable for feature selection. The model's application of the $l_{2,p}$-norm can be expressed as:

$$\begin{aligned} &argmin\, \|X - XWH\|_{2,p}^p \\ &s.t. W.H \geq 0, W^T W = I_l \end{aligned} \tag{2}$$

Choosing different $p$ values significantly impacts the model's performance. Fig 1 presents 3D surface plots for three different norms, showing that both $F$-norm and $l_{2,1}$-norm tend to optimize more towards the origin. However, during the optimization process, the $l_{2,1/2}$-norm is more inclined towards the coordinate axes. Therefore, using the $l_{2,1/2}$-norm to constrain the model effectively eliminates redundant features and selects more discriminative features.

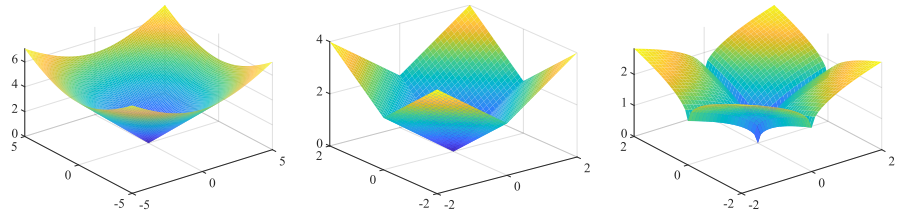

(a) $F$ -norm (b) $l_{2,1}$ -norm (c) $l_{2,1/2}$ -norm

**Fig 1. 3D surface plot of $F$-norm, $l_{2,1}$-norm and $l_{2,1/2}$-norm regularization term.**

## 2.3. Sparsity regularization term of the feature selection matrix

Reference [22] emphasizes the critical role of the feature weight matrix $W$ in the feature selection process and highlights the necessity of introducing appropriate regularization techniques for effectively learning $W$. However, conventional regularization methods each have certain limitations: Although $l_1$-norm regularization can achieve sparsity, it can easily lead to under-fitting in high-dimensional data; while $l_{2,0}$-norm regularization can produce desirable sparsity, its non-convexity, and NP-hard nature render the optimization process extremely challenging. Moreover, $l_{2,1}$-norm regularization often overlooks correlations among features, resulting in limited performance improvements when dealing with highly redundant features in high-dimensional data.

To address these issues, Han et al. [23] proposed an inner product-based regularization method. By continually reducing the inner products between feature vectors during optimization, this approach forces them closer to zero, thereby effectively mitigating feature redundancy. Several empirical studies have confirmed both the efficacy and superiority of the inner product regularization term. For instance, studies reported in references [24] and [25] have demonstrated that features selected by the inner product regularization exhibit significantly lower inter-feature correlations compared to those selected by $l_{2,1}$-norm regularization. Another study [23] showed that incorporating the inner product regularization term into the feature selection process not only outperforms traditional regularization techniques in terms of clustering performance but also achieves exceptional results with fewer selected features. Collectively, these findings indicate that the inner product regularization term helps select more representative and less redundant features, thereby enhancing the overall performance of feature selection. The inner product regularization term for the feature selection matrix $W$ is defined as:

$$\sum_{i,j=1,i\neq j}^{d} < w^i, w^j > \; = \sum_{i,j=1,i\neq j}^{d} w^i {w^j}^T = Tr(1_{d\times d} W W^T) - Tr(W W^T) \tag{3}$$

## 2.4. Adaptive Graph Learning

In the design of existing model, the global structure and constraints on the feature selection matrix have been thoroughly considered. To further enhance the generalizability of the model, local structural information is incorporated, and the most effective way to achieve this is by introducing graph learning [26]. Graph structures can effectively preserve the local neighborhood information of data, and when mapping from the original feature space to a lower-dimensional feature space, they can maintain the geometric structure of the samples [27]. Simply put, if two sample points are close to each other in the original space, they should also remain close in the feature-selected projection space. Mathematically, this can be expressed as:

$$\min_{S} \sum_{i,j=1}^{n} ||W^T x_i - W^T x_j||_2^2 s_{ij} = Tr(W^T X^T L X W) \tag{4}$$

However, real-world data is often affected by noise, which making the $k$-nearest neighbor graph constructed using the aforementioned methods susceptible to inaccuracies. To address this issue, researchers in [28] have proposed adaptive graph learning as an effective solution to the problems of imbalanced neighbors and feature redundancy. Adaptive graph learning dynamically computes the similarity matrix during the optimization process, enabling it to more accurately capture the true relationships between samples without relying on predefined Euclidean or cosine distances. By dynamically adjusting neighbor relationships, adaptive graph learning overcomes the limitations of traditional predefined methods and significantly enhances the model's robustness to noise and adaptability to high-dimensional data.

$$\begin{aligned} \min_{S} & Tr(W^T X^T L X W) + \gamma ||S||_F^2 \\ & s.t. \sum\nolimits_{j=1}^{n} s_{ij} = 1, s_{ij} \geq 0 \end{aligned} \tag{5}$$

Where $L$ is the Laplacian matrix, and $L = D - S$. $S \in R^{n \times n}$represents the similarity matrix of the samples, where the element $s_{ij}$ denotes the similarity between the sample points $x_i$ and $x_j$ . The matrix $S$ can be calculated adaptively, $\gamma$ influences the nearest neighbor number of each sample. $D \in R^{n \times n}$is a diagonal matrix and its diagonal elements are defined as:

$$d_{ii} = \sum\nolimits_{j=1}^{n} s_{ij} \tag{6}$$

# 3. Unsupervised Feature Selection Based on $l_{2,p}$-norm Feature Reconstruction

## 3.1. Model Construction

In constructing the subspace, the $l_{2,p}$-norm is used to flexibly measure the distance between the original samples and the reconstructed samples. The adaptive graph embedding learning takes into account the similarity relationships between samples, preserving the local geometric structure of the data. In addition, by applying an inner product constraint on the feature selection matrix, a more sparse solution can be obtained to help to select a representative subset of features. The final objective

function is expressed as:

$$\begin{aligned} \min ||X - XWH||_{2,p}^{p} + \alpha Tr(W^T X^T LXW) + \\ \beta(Tr(1_{d\times d}WW^T) - Tr(WW^T)) + \gamma||S||_F^2 \\ s.t. W \geq 0, H \geq 0, W^T W = I, \sum_{j=1}^{n} s_{ij} = 1, s_{ij} \geq 0 \end{aligned} \tag{7}$$

Where $\alpha$, and $\beta$ are regularization parameters, and $\gamma$ is a coefficient that can be determined during the optimization process.

## 3.2. Model Solution

The objective function in eq (6) includes three variables, $W$, $H$, and $S$. To improve computational efficiency, this paper employs an alternate optimization method to optimize the objective function, that is, by fixing two variables each time and optimizing the other variable.

Define two Lagrange multipliers, $\theta$ and $\mu$, to ensure the non-negativity of the matrices $W$ and $H$. The resulting Lagrangian function is as follows:

$$\begin{aligned} L(W,H) =& ||X - XWH||_{2,p}^{p} + \alpha Tr(W^T X^T LXW) \\ &+ \beta(Tr(1_{d\times d}WW^T) - Tr(WW^T)) \\ &+ \frac{\lambda}{2}(W^T W - I) + Tr(\theta W^T) + Tr(\mu H^T) \end{aligned} \tag{8}$$

Define a diagonal matrix $U$, with diagonal elements being $u_{ii} = \frac{p}{2||(X-XWH)_i||_2^{2-p}}$.

1. Fix $H$, $S$, and Update $W$: By taking the partial derivative of eq ( 8) with respect to $W$, the following formula can be obtained:

$$\begin{aligned} \frac{\partial L}{\partial W} =& - X^T UXH^T + X^T UXWHH^T + \alpha X^T LXW + \beta(WW^T W - W) \\ &+ \lambda(1_{d\times d}W - W) + \theta \end{aligned} \tag{9}$$

By using the Karush–Kuhn–Tucker (KKT) conditions $\theta_{ij}W_{ij} = 0$, the obtained formula is as follows:

$$\begin{aligned} (-X^T UXH^T + X^T UXWHH^T + \alpha X^T LXW \\ +\beta(WW^T W - W) + \lambda(1_{d\times d}W - W))_{ij} W_{ij} = 0 \end{aligned} \tag{10}$$

Thus, the update rule for $W$ is as follows:

$$W_{ij} \leftarrow W_{ij} \frac{\left[XUX^T H^T + \alpha X^T SXW + \beta W + \lambda W\right]_{ij}}{\left[XUX^T WHH^T + \alpha X^T DXW + \beta WW^T W + \lambda 1_{d\times d}W\right]_{ij}} \tag{11}$$

2.Fix $W$, $S$, and Update $H$: By taking the partial derivative of eq (8) with respect to $H$, the following formula can be obtained:

$$\frac{\partial L}{\partial H} = -W^T X^T UX + W^T X^T UXWH^T + \mu \tag{12}$$

By using the Karush–Kuhn–Tucker (KKT) conditions $\mu_{ij}H_{ij} = 0$, the obtained formula is as follows:

$$(-W^T X^T UX + W^T X^T UXWH^T)_{ij} H_{ij} = 0 \tag{13}$$

Thus, the update rule for $H$ is as follows:

$$H_{ij} \leftarrow H_{ij} \frac{\left[W^T X^T U X\right]_{ij}}{\left[W^T X^T U X W H^T\right]_{ij}} \tag{14}$$

3.Fix $W$, $H$, and Update $S$: By taking the partial derivative of eq (8) with respect to $S$, the following formula can be obtained:

$$\begin{aligned} \min_S \sum_{i,j=1}^{n} (\alpha ||W^T x_i - W^T x_j||_2^2 s_{ij} + \gamma s_{ij}^2) \\ s.t. \sum\nolimits_{j=1}^{n} s_{ij} = 1, s_{ij} \geq 0 \end{aligned} \tag{15}$$

Denote $d_{ij} = ||W^T x_i - W^T x_j||_2^2$,so we can transform eq (14) to a vector form as

$$\begin{aligned} \min_{s_i^T \mathbf{1}=1, s_i \geq 0} ||s_i + \frac{\alpha}{2\gamma} d_i||_2^2 \\ s.t. \sum\nolimits_{j=1}^{n} s_{ij} = 1, s_{ij} \geq 0 \end{aligned} \tag{16}$$

Introduce Lagrange multipliers $\omega$ and $\mu$ to construct the Lagrangian function:

$$\mathcal{L}(s_i, \omega, \varphi_i) = ||s_i + \frac{\alpha}{2\gamma} d_i||_2^2 - \omega(s_i^T \mathbf{1} - 1) - \varphi_i^T s_i \tag{17}$$

According to the KKT conditions, the optimal solution is obtained.

$$s_{ij} = (-\frac{\alpha d_{ij}}{2\varepsilon_i} + \omega)_+ \tag{18}$$

In unsupervised feature selection algorithms, preserving the local geometric manifold structure of the data tends to be more effective than preserving the global structure. Therefore, only neighboring points $k$ are considered to construct the similarity matrix. The optimal solution for $\gamma$ can be represented as the average of all $\gamma_i$ [29]. Assuming $d_{i1}, d_{i2}, \ldots, d_{in}$ is sorted from smallest to largest and satisfies the condition.Because $s_i$ satisfies $s_{ik} > 0 \geq s_{i,k+1}$, we have then we have:

$$\begin{cases} s_{ik} > 0 \Rightarrow -\frac{\alpha d_{ik}}{2\varepsilon_i} + \omega > 0 \\ s_{i,k+1} \leq 0 \Rightarrow -\frac{\alpha d_{i,k+1}}{2\varepsilon_i} + \omega \leq 0. \end{cases} \tag{19}$$

According to eq (18) and the constraint $s_i^T 1 = 1$ we have

$$\sum_{j=1}^{k} (-\frac{\alpha d_{ij}}{2\gamma_i} + \omega) = 1 \Rightarrow \omega = \frac{1}{k} + \frac{\alpha}{2k\gamma_i} \sum_{i=1}^{k} d_{ij} \tag{20}$$

By substituting the value of $\omega$ in eq (19) into eq (18), we have

$$\frac{\alpha}{2} \left( k d_{ik} - \sum_{j=1}^{k} d_{ij} \right) < \gamma_i \leq \frac{\alpha}{2} \left( k d_{i,k+1} - \sum_{j=1}^{k} d_{ij} \right) \tag{21}$$

Therefore, in order to obtain an optimal solution of $s_i$ that has exact $k$ nonzero values, we set $\gamma_i$ to be

$$\gamma_i = \frac{\alpha}{2} \left( k d_{i,k+1} - \sum_{j=1}^{k} d_{ij} \right) \tag{22}$$

and then the overall $\gamma$ is set to the mean of $\gamma_i$ as

$$\gamma = \frac{1}{n}\sum_{i=1}^{n}(\frac{\alpha k}{2}d_{i,k+1} - \frac{\alpha}{2}\sum_{j=1}^{k} d_{ij}) \tag{23}$$

Finally, substitute eq (22) into eq (17), and consider only $k$ neighboring points to construct the similarity matrix. In summary, the solution can be obtained by solving as

$$s_{ij} = \begin{cases} \frac{d_{i,k+1}-d_{ij}}{\alpha k d_{i,k+1} - \alpha\sum_{j=1}^{k} d_{ij}}, j \leq k \\ 0, j \geq k+1 \end{cases} \tag{24}$$

**Algorithm 1:** NFRFS

**Input:** Date matrix $X$, the coefficient $\alpha$, $\beta$, and $p$, the dimension of the subspace $l$, select feature number $m$

**Output:** Calculate and sort $\|w_i\|_2$ in the descending order, then select the top $m$ ranked features as the results of feature selection.

Initialize $t = 0$, $W$, $H$, maxIter
while $t \leq$ maxIter do
update $W$ by eq (11)
update $H$ by eq (14)
update $S$ by eq (24)
**end while**

## 3.3. Convergence of Algorithm

In this section, we present the convergence analysis of the proposed NFRFS algorithm. Algorithm 1 solves equation (7) by iteratively updating the matrices $W$, $H$, and $S$. Due to the closed-form expression of $s_i$, equation (24) is guaranteed to be nonincreasing when optimizing $S$ while keeping $W$ and $H$ fixed. Subsequently, we verify that the objective function monotonically decreases under the updating rule specified in equation (11). Since the update of the matrix $W$ involves the $\ell_{2,p}$-norm, it is necessary to introduce and reference the following two lemmas in the proof. [30]

**Lemma 1:** If $\phi(t) = \frac{2}{2-p}t^{-\frac{p}{2-p}}$ when $p \in (0,1)$ and $t > 0$, therefore, $\phi(t) \leq 0$

**Lemma 2:** Assume $g_i^t$ and $g_i^{t+1}$ as the $i$-th row of matrices $G_t$ and $G_{t+1}$, respectively, thus for $p \in (0,1]$we have:

$$\|g_i^{t+1}\|_2^p - \frac{p}{2}\left(\frac{\|g_i^{t+1}\|_2^2}{\|g_i^t\|_2^{2-p}}\right) \leq \|g_i^t\|_2^p - \frac{p}{2}\left(\frac{\|g_i^t\|_2^2}{\|g_i^t\|_2^{2-p}}\right) \tag{25}$$

$$\Rightarrow \sum_{i=1}^{r}\left(\|g_i^{t+1}\|_2^p - \frac{p}{2}\left(\frac{\|g_i^{t+1}\|_2^2}{\|g_i^t\|_2^{2-p}}\right)\right) \leq \sum_{i=1}^{r}\left(\|g_i^t\|_2^p - \frac{p}{2}\left(\frac{\|g_i^t\|_2^2}{\|g_i^t\|_2^{2-p}}\right)\right) \tag{26}$$

**Theorem 1.** For $0 < p \leq 1$, algorithm 1 monotonically decreases the objective value in (7) until convergence.

**Proof.** We deduce the following formula from Eq. (23):

$$\begin{aligned} W^{(t+1)} = \arg\min_{W} \Big\{ &\|X - XW^{(t)}H^{(t)}\|_{2,p} + \alpha \mathrm{Tr}\left((W^{(t)})^T X^T L X W^{(t)}\right) \\ &+\beta\left(\mathrm{Tr}\left(1_{d\times d}W^{(t)}(W^{(t)})^T\right) - \mathrm{Tr}\left(W^{(t)}(W^{(t)})^T\right)\right)\Big\} \end{aligned} \tag{27}$$

Hence, we have:

$$\begin{aligned}
&\|X - XW^{(t+1)}H^{(t)}\|_{2,p} + \alpha \mathrm{Tr}\left((W^{(t+1)})^T X^T L X W^{(t+1)}\right) \\
&+ \beta\left(\mathrm{Tr}\left(1_{d\times d} W^{(t+1)}(W^{(t+1)})^T\right) - \mathrm{Tr}\left(W^{(t+1)}(W^{(t+1)})^T\right)\right) \\
\leq &\|X - XW^{(t)}H^{(t)}\|_{2,p} + \alpha \mathrm{Tr}\left((W^{(t)})^T X^T L X W^{(t)}\right) \\
&+ \beta\left(\mathrm{Tr}\left(1_{d\times d} W^{(t)}(W^{(t)})^T\right) - \mathrm{Tr}\left(W^{(t)}(W^{(t)})^T\right)\right)
\end{aligned} \tag{28}$$

Meanwhile, the following two equations hold.

$$\begin{aligned}
&\|X - XW^{(t)}H^{(t)}\|_{2,p} \\
=&Tr\{(X - XW^{(t)}H^{(t)})^T U^{(t)}(X - XW^{(t)}H^{(t)})\} \\
=&\sum_i \frac{p}{2}\frac{\|(X - XW^{(t)}H^{(t)})_i\|_2^2}{\|(X - XW^{(t)}H^{(t)})_i\|_2^{2-p}}
\end{aligned} \tag{29}$$

$$\begin{aligned}
&\|X - XW^{(t+1)}H^{(t)}\|_{2,p} \\
=&Tr\{(X - XW^{(t+1)}H^{(t)})^T U^{(t)}(X - XW^{(t+1)}H^{(t)})\} \\
=&\sum_i \frac{p}{2}\frac{\|(X - XW^{(t+1)}H^{(t)})_i\|_2^2}{\|(X - XW^{(t+1)}H^{(t)})_i\|_2^{2-p}}
\end{aligned} \tag{30}$$

Therefore, it is easy to get

$$\begin{aligned}
&\sum_i \frac{p}{2}\frac{\|(X - XW^{(t+1)}H^{(t)})_i\|_2^2}{\|(X - XW^{(t)}H^{(t)})_i\|_2^{2-p}} + \alpha \mathrm{Tr}\left((W^{(t+1)})^T X^T L X W^{(t+1)}\right) \\
&+ \beta\left(\mathrm{Tr}\left(1_{d\times d} W^{(t+1)}(W^{(t+1)})^T\right) - \mathrm{Tr}\left(W^{(t+1)}(W^{(t+1)})^T\right)\right) \\
\leq &\sum_i \frac{p}{2}\frac{\|(X - XW^{(t)}H^{(t)})_i\|_2^2}{\|(X - XW^{(t)}H^{(t)})_i\|_2^{2-p}} + \alpha \mathrm{Tr}\left((W^{(t)})^T X^T L X W^{(t)}\right) \\
&+ \beta\left(\mathrm{Tr}\left(1_{d\times d} W^{(t)}(W^{(t)})^T\right) - \mathrm{Tr}\left(W^{(t)}(W^{(t)})^T\right)\right)
\end{aligned} \tag{31}$$

$$\begin{aligned}
\Rightarrow &\sum_i \frac{p}{2}\frac{\|(X - XW^{(t+1)}H^{(t)})_i\|_2^2}{\|(X - XW^{(t)}H^{(t)})_i\|_2^{2-p}} + \alpha \mathrm{Tr}\left((W^{(t+1)})^T X^T L X W^{(t+1)}\right) \\
&+ \beta\left(\mathrm{Tr}\left(1_{d\times d} W^{(t+1)}(W^{(t+1)})^T\right) - \mathrm{Tr}\left(W^{(t+1)}(W^{(t+1)})^T\right)\right) \\
&- \sum_i \|(X - XW^{(t+1)}H^{(t)})_i\|_2^p + \sum_i \|(X - XW^{(t+1)}H^{(t)})_i\|_2^p \\
\leq &\sum_i \frac{p}{2}\frac{\|(X - XW^{(t)}H^{(t)})_i\|_2^2}{\|(X - XW^{(t)}H^{(t)})_i\|_2^{2-p}} + \alpha \mathrm{Tr}\left((W^{(t)})^T X^T L X W^{(t)}\right) \\
&+ \beta\left(\mathrm{Tr}\left(1_{d\times d} W^{(t)}(W^{(t)})^T\right) - \mathrm{Tr}\left(W^{(t)}(W^{(t)})^T\right)\right) \\
&- \sum_i \|((X - XW^{(t)}H^{(t)})_i\|_2^p + \sum_i \|(X - XW^{(t)}H^{(t)})_i\|_2^p
\end{aligned} \tag{32}$$

$$
\begin{aligned}
&\Rightarrow \beta\left(\mathrm{Tr}\left(1_{d\times d}W^{(t+1)}(W^{(t+1)})^T\right)-\mathrm{Tr}\left(W^{(t+1)}(W^{(t+1)})^T\right)\right)\\
&\quad+\sum_i\|(X-XW^{(t+1)}H^{(t)})_i\|_2^p\\
&\quad-\left\{\sum_i\|(X-XW^{(t+1)}H^{(t)})_i\|_2^p-\sum_i\frac{p}{2}\frac{\|(X-XW^{(t+1)}H^{(t)})_i\|_2^2}{\|(X-XW^{(t)}H^{(t)})_i\|_2^{2-p}}\right\}\\
&\leq\beta\left(\mathrm{Tr}\left(1_{d\times d}W^{(t)}(W^{(t)})^T\right)-\mathrm{Tr}\left(W^{(t)}(W^{(t)})^T\right)\right)\\
&\quad+\sum_i\|(X-XW^{(t)}H^{(t)})_i\|_2^p\\
&\quad-\left\{\sum_i\|(X-XW^{(t)}H^{(t)})_i\|_2^p-\sum_i\frac{p}{2}\frac{\|(X-XW^{(t)}H^{(t)})_i\|_2^2}{\|(X-XW^{(t)}H^{(t)})_i\|_2^{2-p}}\right\}
\end{aligned}
\tag{33}
$$

It is proved in Lemma 2 that

$$
\begin{aligned}
&\sum_i\left\{\|(X-XW^{(t+1)}H^{(t)})_i\|_2^p-\frac{p}{2}\frac{\|(X-XW^{(t+1)}H^{(t)})_i\|_2^2}{\|(X-XW^{(t)}H^{(t)})_i\|_2^{2-p}}\right\}\\
&\leq\sum_i\left\{\|(X-XW^{(t)}H^{(t)})_i\|_2^p-\frac{p}{2}\frac{\|(X-XW^{(t)}H^{(t)})_i\|_2^2}{\|(X-XW^{(t)}H^{(t)})_i\|_2^{2-p}}\right\}
\end{aligned}
\tag{34}
$$

Thus, we have

$$
\begin{aligned}
&\sum_i\|(X-XW^{(t+1)}H^{(t)})_i\|_2^p+\alpha\mathrm{Tr}\left((W^{(t+1)})^TX^TLXW^{(t+1)}\right)\\
&\quad+\beta\left(\mathrm{Tr}\left(1_{d\times d}W^{(t+1)}(W^{(t+1)})^T\right)-\mathrm{Tr}\left(W^{(t+1)}(W^{(t+1)})^T\right)\right)\\
&\leq\sum_i\|(X-XW^{(t)}H^{(t)})_i\|_2^p+\alpha\mathrm{Tr}\left((W^{(t)})^TX^TLXW^{(t)}\right)\\
&\quad+\beta\left(\mathrm{Tr}\left(1_{d\times d}W^{(t)}(W^{(t)})^T\right)-\mathrm{Tr}\left(W^{(t)}(W^{(t)})^T\right)\right)
\end{aligned}
\tag{35}
$$

$$
\begin{aligned}
&\Rightarrow\|X-XW^{(t+1)}H^{(t)}\|_{2,p}+\alpha\mathrm{Tr}\left((W^{(t+1)})^TX^TLXW^{(t+1)}\right)\\
&\quad+\beta\left(\mathrm{Tr}\left(1_{d\times d}W^{(t+1)}(W^{(t+1)})^T\right)-\mathrm{Tr}\left(W^{(t+1)}(W^{(t+1)})^T\right)\right)\\
&\leq\|X-XW^{(t)}H^{(t)}\|_{2,p}+\alpha\mathrm{Tr}\left((W^{(t)})^TX^TLXW^{(t)}\right)\\
&\quad+\beta\left(\mathrm{Tr}\left(1_{d\times d}W^{(t)}(W^{(t)})^T\right)-\mathrm{Tr}\left(W^{(t)}(W^{(t)})^T\right)\right)
\end{aligned}
\tag{36}
$$

When fixing $W^{(t+1)}$ to update $H^{(t+1)}$ , we have the following inequality:

$$
\begin{aligned}
&\|X-XW^{(t+1)}H^{(t+1)}\|_{2,1}+\alpha\mathrm{Tr}\left((W^{(t+1)})^TX^TLXW^{(t+1)}\right)\\
&\quad+\beta\left(\mathrm{Tr}\left(1_{d\times d}W^{(t+1)}(W^{(t+1)})^T\right)-\mathrm{Tr}\left(W^{(t+1)}(W^{(t+1)})^T\right)\right)\\
&\leq\|X-XW^{(t+1)}H^{(t)}\|_{2,1}+\alpha\mathrm{Tr}\left((W^{(t+1)})^TX^TLXW^{(t+1)}\right)\\
&\quad+\beta\left(\mathrm{Tr}\left(1_{d\times d}W^{(t+1)}(W^{(t+1)})^T\right)-\mathrm{Tr}\left(W^{(t+1)}(W^{(t+1)})^T\right)\right)
\end{aligned}
\tag{37}
$$

By integrating eq (36) with eq (37), we obtain

$$\begin{aligned}
&\|X - XW^{(t+1)}H^{(t+1)}\|_{2,1} + \alpha \mathrm{Tr}\left((W^{(t+1)})^T X^T L X W^{(t+1)}\right) \\
&+ \beta\left(\mathrm{Tr}\left(1_{d\times d} W^{(t+1)}(W^{(t+1)})^T\right) - \mathrm{Tr}\left(W^{(t+1)}(W^{(t+1)})^T\right)\right) \\
\leq &\|X - XW^{(t)}H^{(t)}\|_{2,1} + \alpha \mathrm{Tr}\left((W^{(t)})^T X^T L X W^{(t)}\right) \\
&+ \beta\left(\mathrm{Tr}\left(1_{d\times d} W^{(t)}(W^{(t)})^T\right) - \mathrm{Tr}\left(W^{(t)}(W^{(t)})^T\right)\right)
\end{aligned} \tag{38}$$

So, it is sensible to believe that the objective function decreases monotonically during the optimization process.

### 3.4. Complexity Analysis

This section show the analysis of the time complexity and space complexity of the NFRFS algorithm. Let $n$ represent the total number of samples, $d$ represent the number of sample features, $c$ represent the number of sample classes in the dataset, $l$ represent the dimension of the subspace, and $t$ represent the maximum number of iterations. According to eq (11), the time complexity for updating matrix $W$ is $O(n^2d + nd + dl)$, according eq (14), the time complexity for updating matrix $H$ is $O(nd + d^2n)$, and according to eq (24), the time complexity for updating matrix $S$ is $O(n^2)$. Since the dimension of the subspace is less than the number of samples and the dimensionality of the data, the overall time complexity of the algorithm is $O(t(n^2d + d^2n))$. Throughout the algorithm, we need to store data and related variables $O(nd + dl)$. The space complexity of constructing the similarity matrix $S$ based on adaptive graph learning is $O(n^2)$. So the space complexity of the algorithm is $O(n^2 + nd)$.

Table 2 visually lists the time complexity of the comparison algorithm and the time complexity of our algorithm.

**Table 2. Computational complexity of all methods.**

| **Methods** | **Computational complexity** |
|---|---|
| LS | $O(n^2d)$ |
| MCFS | $O(d^3 + n^2m + d^2n)$ |
| SPFS | $O(n^2d)$ |
| VSCDFS | $O(d^2)$ |
| AUFS | $O(d^3)$ |
| GLUFS | $O(max(n^3, d^3))$ |
| HSL | $O(d^3 + ndm + 1)$ |
| LRPFS | $O(dn^2 + nd^2)$ |
| RAFG | $O(d^3 + n^3 + n^2c + ndc)$ |
| NFRFS | $O(n^2d + d^2n)$ |

## 4. Experiment

### 4.1 Datasets

We evaluate the effectiveness of the feature selection model on 14 datasets, spanning five different fields, including six face image datasets (Yale, warpPIE10P, warpAR10P, ORL, JAFFE, ATT40), three biological datasets (lung, TOX-171, Lung_small), one object image dataset (COIL20), one speech signal dataset (Isolet), and two text

datasets (PCMAC, RELATHE). Details about the number of samples, features, classes, types, and sources are provided in table 3.

**Table 3. Detail introduction to datasets.**

| Dataset | Samples | Features | Classes | Type | Source |
|---|---|---|---|---|---|
| Yale | 165 | 1024 | 15 | Face Image | http://www.cad.zju.edu.cn/home/dengcai/Data/data.html |
| lung | 203 | 3312 | 5 | Biological | https://jundongl.github.io/scikit-feature/datasets.html |
| COIL20 | 1440 | 1024 | 20 | Object Image | http://www.cad.zju.edu.cn/home/dengcai/Data/data.html |
| warpPIE10P | 210 | 2420 | 10 | Face Image | https://jundongl.github.io/scikit-feature/datasets.html |
| warpAR10P | 130 | 2400 | 10 | Face Image | https://jundongl.github.io/scikit-feature/datasets.html |
| ORL | 400 | 1024 | 40 | Face Image | https://jundongl.github.io/scikit-feature/datasets.html |
| JAFFE | 213 | 256 | 10 | Face Image | [31] |
| ATT40 | 400 | 1024 | 40 | Face Image | [32] |
| TOX-171 | 171 | 5748 | 4 | Biological | https://jundongl.github.io/scikit-feature/datasets.html |
| Isolet | 1560 | 617 | 26 | Speech signal | https://jundongl.github.io/scikit-feature/datasets.html |
| binalpha | 1404 | 320 | 36 | Handwritten Digit | [33] |
| Lung_small | 73 | 325 | 7 | Biological | https://jundongl.github.io/scikit-feature/datasets.html |
| PCMAC | 1943 | 3289 | 2 | Text | https://jundongl.github.io/scikit-feature/datasets.html |
| RELATHE | 1427 | 4322 | 2 | Text | https://jundongl.github.io/scikit-feature/datasets.html |

## 4.2. Compared methods

To validate the effectiveness of the proposed approach in unsupervised feature selection, the proposed approach is compared with a baseline method that performs clustering with all the original features and nine other representative existing unsupervised feature selection methods.

LS [9]: Laplacian Score (LS) uses the local geometric information of data to select features, and calculates the score of each feature separately.

MCFS [14]: Multi-cluster feature selection (MCFS) is a multi-cluster feature selection method that initially performs spectral analysis followed by feature selection via sparse regression.

SPFS [34]: Structured learning for unsupervised feature selection with high-order matrix factorization (SPFS) integrates local and global structures into a unified framework and formulates the framework as a form of high-order matrix decomposition.

VSCDFS [35]: Unsupervised feature selection based on variance-covariance subspace distance (VSCDFS) selects a representative feature subset using variance-covariance information of the feature space.

AUFS [36]: Adaptive unsupervised feature selection with robust graph regularization (AUFS) performs unsupervised feature selection by minimizing an objective function that includes self-representation reconstruction error, $l_{2,p}$-norm regularization term, and robust graph regularization term.

GLUFS [37]: It integrates the construction of similarity matrices and feature selection into a unified framework, introducing a sparse learning strategy with $l_{2,0}$-norm constraint.

HSL [38]: Unsupervised feature selection with high-order similarity learning (HSL) simultaneously learns the projection matrix, first-order similarity information, and higher-order similarity information within a unified framework.

LRPFS [39]: Unsupervised Feature Selection with Latent Relationship Penalty Term (LRPFS) explicitly assigns attribute scores to each sample based on its unique

importance in the clustering results.

RAFG [40]: Adaptive and flexible $l_1$-norm graph embedding for unsupervised feature selection (RAFG) incorporates the $l_{2,1}$-norm into the elastic regression term and characterizes clustering distributions through adaptive $l_1$-norm graph learning with consistent embeddings.

## 4.3. Evaluation Methodology

To verify the clustering performance of the algorithm, this article adopts two evaluation indicators, namely cluster accuracy (ACC) [41] and Normalized Mutual Information (NMI) [42]. Both values are within the range of [0, 1]. The higher the values of ACC and NMI, the better the clustering effect and the more representative the selected feature subset.

1. ACC

$$ACC = \frac{1}{n}\sum_{i=1}^{n}\delta(w_i, map(m_i))$$

Where $w_i$ denotes the ideal label, $m_i$ represents the predicted label, $map(\cdot)$ denotes the optimal mapping function, and $\delta(\cdot)$ represents the indicator function. If $a = b$ , then $\delta(a, b) = 1$ , otherwise $\delta(a, b) = 0$.

2. NMI

$$NMI = \frac{I(w, m)}{\sqrt{H(w)H(m)}}$$

Where $w$ denotes the ideal label, $m$ represents the predicted label, $I(\cdot)$ denotes the mutual information, and $H(\cdot)$ represents the information entropy. NMI ranges from 0 to 1. NMI is 1 when the two sets are identical and 0 when they are independent. In general, higher ACC values and higher NMI values indicate better performance.

## 4.4. Experimental settings

It is necessary to specify several parameter values for the NFRFS method proposed in this paper and other comparison methods before starting the experiment. The regularization parameters of all algorithms are set within the range $\{10^{-6}, 10^{-4}, 10^{-2}, 1, 10^2, 10^4, 10^6\}$ using the grid search method, and the best results of all algorithms are recorded. The number of selected features in the dataset is $\{20, 40, 60, \cdots, 160, 180, 200\}$. The dimension of the subspace $l$ is set to $\{\frac{d}{3}, \frac{d}{2}, \frac{2d}{3}\}$. The K-means algorithm is used to cluster the data points formed by the selected features to evaluate different methods. Considering that the K-means algorithm is sensitive to initialization, the experiment repeats the K-means algorithm 20 times to eliminate the influence of initial points on the clustering effect.

## 4.5. Analysis of Experimental Results

Table 4 and 5 respectively present the best clustering accuracy (ACC) and normalized mutual information (NMI) scores achieved by NFRFS and other comparative algorithms on 14 datasets, along with the corresponding standard deviations (STD). The highest values among different algorithms for the same dataset are highlighted in bold black font in the tables. The specific results are shown in the tables.

As can be seen from table 4 and 5, within the 14 datasets comprising six diverse data types, the ACC and NMI of the NFRFS algorithm significantly exceed those of the baselines using all the original features. This indicates that the NFRFS algorithm is capable of achieving superior ACC and NMI with a relatively smaller number of

selected features, which effectively validates the efficacy of the NFRFS algorithm in enhancing clustering performance.

Across the 14 datasets tested, NFRFS achieves the highest ACC and NMI scores on all but three datasets (COIL20, binalpha, and RELATHE). However, for the COIL20, binalpha, and RELATHE datasets, although the clustering performance of NFRFS is slightly inferior, it is very close to the best clustering results achieved by other methods. On the COIL20 dataset, the ACC of the NFRFS algorithm is marginally lower than that of AUFS and HSL. For the binalpha dataset, both the ACC and NMI of NFRFS acquire sub-optimal values. Notably, on the RELATHE dataset, the NMI performance of NFRFS remains higher than that of all other algorithms.

It can be observed from table 4 that the improvement achieved by NFRFS on the warpPIE10P dataset is the most remarkable. Specifically, it has increased by 4.26% compared to the second-best algorithm and by 32.5% compared to the method that employs all features for clustering. As shown in table 5, the enhancement of NFRFS on the PCMAC dataset is the most prominent. The NMI of the other eleven algorithms is all below 10%, while the performance of NFRFS reaches 12.18%. Compared with the SPFS algorithm, the proposed NFRFS algorithm demonstrates superior performance. In particular, on the lung, warpPIE10P, and TOX-171 datasets, the ACC has been increased by more than 9%, and on the Yale and TOX-171 datasets, the NMI has been increased by more than 12%. This is because NFRFS adopts adaptive graph regularization and utilizes the robust $l_{2,p}$-norm loss function. Consequently, NFRFS has an advantage in feature selection performance.

**Table 4. Best ACC for different methods on different datasets (mean±std%).**

| Dataset | baseline | LS | MCFS | SPFS | VSCDFS | AUFS | GLUFS | HSL | LRPFS | RAFG | NFRFS |
|---|---|---|---|---|---|---|---|---|---|---|---|
| Yale | 38.64±3.61 | 36.94±2.17 | 40.61±3.33 | 39.36±2.36 | 37.12±2.28 | 46.70±3.14 | 45.97±3.90 | 49.70±3.43 | 38.97±2.15 | 50.03±3.61 | **50.39±3.18** |
| lung | 72.46±10.20 | 57.91±7.48 | 72.02±7.57 | 75.37±6.71 | 60.47±7.43 | 79.68±4.52 | 81.55±10.03 | 79.85±3.94 | 63.87±1.40 | 77.64±3.29 | **84.04±4.14** |
| COIL20 | 59.17±3.98 | 53.89±3.34 | 60.92±3.52 | 68.27±2.24 | 60.56±4.41 | 70.26±1.82 | 68.68±2.86 | **71.05±3.32** | 68.91±3.26 | 62.14±2.40 | 69.94±2.25 |
| warpPIE10P | 26.24±2.03 | 44.71±3.00 | 28.86±2.56 | 48.52±3.27 | 25.79±1.21 | 54.48±1.26 | 37.21±2.76 | 45.90±0.99 | 34.17±1.53 | 52.45±1.96 | **58.74±3.96** |
| warpAR10P | 23.58±3.94 | 33.08±3.08 | 30.54±3.23 | 48.92±2.86 | 26.88±3.39 | 40.92±1.72 | 40.23±2.64 | 43.15±3.30 | 43.81±2.97 | 42.65±2.69 | **51.62±3.51** |
| ORL | 51.79±3.37 | 40.09±2.20 | 52.71±3.02 | 51.01±2.26 | 48.21±2.97 | 53.70±1.92 | 54.43±2.90 | 54.89±2.24 | 51.89±2.21 | 55.42±2.40 | **58.66±2.37** |
| JAFFE | 67.28±6.18 | 66.38±6.15 | 70.26±6.35 | 78.22±4.30 | 69.86±7.89 | 80.80±3.52 | 81.20±3.77 | 80.00±4.49 | 77.96±4.11 | 81.62±2.97 | **83.43±1.90** |
| ATT40 | 51.28±3.86 | 49.16±2.80 | 53.19±3.49 | 55.48±3.14 | 49.56±3.00 | 58.66±2.75 | 55.85±2.89 | 55.18±2.65 | 54.01±2.35 | 55.39±3.05 | **59.31±2.37** |
| TOX-171 | 43.65±3.14 | 41.29±2.48 | 46.90±3.31 | 47.78±1.78 | 43.04±2.51 | 43.77±1.32 | 57.60±0.70 | 53.95±2.98 | 43.10±1.54 | 49.15±3.99 | **58.89±1.30** |
| Isolet | 57.35±3.44 | 58.09±2.72 | 57.73±2.80 | 67.27±2.25 | 61.52±2.97 | 70.72±1.58 | 65.94±2.24 | 60.32±2.38 | 65.24±2.03 | 47.87±2.09 | **71.83±3.31** |
| binalpha | 41.17±1.87 | 39.56±1.51 | 41.66±1.44 | 42.34±1.75 | 39.70±2.08 | 43.82±2.12 | 43.39±1.35 | 43.31±1.72 | 42.64±1.66 | **45.47±1.65** | 45.08±1.36 |
| lung_small | 67.81±7.42 | 67.74±5.56 | 69.93±6.83 | 79.59±5.41 | 65.00±6.49 | 82.26±5.47 | 80.00±5.09 | 78.15±5.29 | 81.92±5.02 | 79.18±5.49 | **83.97±5.55** |
| PCMAC | 50.48±0.50 | 50.63±0.00 | 50.49±0.00 | 56.82±0.00 | 50.54±0.00 | 58.17±0.77 | 51.47±1.07 | 51.94±0.40 | 58.17±0.75 | 56.12±0.21 | **58.84±0.08** |
| RELATHE | 54.45±5.44 | 54.67±0.00 | 54.89±0.70 | 59.06±0.12 | 54.66±0.00 | 57.52±1.56 | 54.53±0.11 | 56.44±0.39 | **61.21±0.75** | 58.85±0.26 | 59.78±0.00 |

**Table 5. Best NMI for different methods on different datasets (mean±std%).**

| Dataset | baseline | LS | MCFS | SPFS | VSCDFS | AUFS | GLUFS | HSL | LRPFS | RAFG | NFRFS |
|---|---|---|---|---|---|---|---|---|---|---|---|
| Yale | 46.48±2.88 | 44.15±1.67 | 49.23±2.79 | 46.17±2.27 | 44.35±1.92 | 56.34±2.87 | 51.37±1.67 | 57.39±7.79 | 46.23±1.26 | 57.49±2.81 | **59.10±2.15** |
| lung | 60.37±5.38 | 47.04±3.14 | 59.87±5.85 | 65.04±0.88 | 53.47±5.36 | 64.74±1.30 | 66.49±4.01 | 64.36±1.89 | 51.66±0.98 | 65.87±1.34 | **66.78±3.16** |
| COIL20 | 75.58±1.64 | 70.53±1.45 | 74.25±2.04 | 79.73±1.35 | 75.13±1.31 | 79.76±1.02 | 78.65±1.29 | **80.91±1.45** | 78.05±1.29 | 76.82±0.86 | 80.04±1.04 |
| warpPIE10P | 25.36±3.18 | 50.09±3.36 | 30.74±3.57 | 56.41±2.54 | 22.62±2.18 | 59.87±2.10 | 39.78±3.42 | 48.19±2.30 | 26.31±1.31 | 56.87±1.84 | **63.10±1.47** |
| warpAR10P | 20.28±5.42 | 35.23±2.91 | 29.47±2.78 | 51.68±1.67 | 22.05±3.52 | 43.57±1.67 | 42.49±3.60 | 44.77±2.39 | 47.41±3.06 | 44.66±2.73 | **53.18±2.71** |
| ORL | 74.26±1.82 | 63.93±1.46 | 74.81±1.71 | 72.59±1.04 | 71.68±1.32 | 74.76±1.20 | 75.82±1.19 | 75.59±1.59 | 73.10±1.21 | 76.23±1.63 | **78.19±1.05** |
| JAFFE | 73.14±3.55 | 71.27±3.52 | 75.77±3.26 | 82.39±1.68 | 76.68±3.62 | 82.32±2.04 | 82.75±1.78 | 83.26±2.65 | 81.37±1.79 | 83.05±2.63 | **84.67±1.50** |
| ATT40 | 74.02±1.79 | 72.23±1.39 | 75.30±1.56 | 75.94±1.57 | 72.41±1.63 | 78.13±0.95 | 76.32±1.27 | 76.13±0.61 | 73.69±0.87 | 76.20±0.68 | **78.53±1.31** |
| TOX-171 | 15.87±4.44 | 16.44±1.33 | 22.69±4.12 | 23.48±1.15 | 12.19±1.53 | 14.97±0.96 | 30.01±0.77 | 34.52±3.69 | 13.49±1.26 | 34.40±0.88 | **36.96±1.20** |
| Isolet | 75.07±1.71 | 74.14±1.14 | 75.29±1.18 | 77.98±0.87 | 75.86±1.29 | 80.01±1.09 | 78.69±1.07 | 73.99±0.69 | 78.00±0.90 | 64.74±0.82 | **81.58±0.89** |
| binalpha | 57.71±0.87 | 55.85±1.24 | 58.29±0.66 | 57.58±0.67 | 55.25±1.03 | 59.05±0.85 | 58.53±0.76 | 59.19±0.51 | 58.28±0.90 | **60.64±0.76** | 59.68±0.93 |
| lung_small | 65.15±7.16 | 64.70±4.42 | 66.62±5.86 | 74.48±3.34 | 62.72±4.66 | 76.61±4.23 | 74.52±3.14 | 74.30±3.39 | 77.39±5.08 | 73.32±3.01 | **78.36±4.33** |
| PCMAC | 0.04±0.03 | 1.24±1.09 | 0.01±0.00 | 3.09±1.43 | 1.91±0.35 | 4.71±0.00 | 1.34±0.00 | 4.38±0.43 | 2.32±0.00 | 4.69±1.13 | **12.18±0.00** |
| RELATHE | 0.22±0.21 | 0.96±0.78 | 1.03±0.65 | 9.39±0.56 | 1.69±0.76 | 6.52±0.11 | 0.48±0.33 | 4.43±2.71 | 9.16±0.20 | 5.87±1.04 | **9.46±0.01** |

Fig 2 and 3 show the relationship between the number of features selected by 11 unsupervised clustering methods on 14 datasets and the best accuracy (ACC) and normalized mutual information (NMI). The horizontal axis represents the number of selected features, and the vertical axis represents ACC and NMI. Compared with direct K-means clustering, NFRFS can achieve a relatively high performance even with a smaller number of selected features. Overall, with the increase in the number of selected features, the ACC and NMI curves of NFRFS first ascend and then descend. This is because real-world datasets usually contain some discriminative features and a large number of noisy features. When very few features are selected, only a part of the discriminative features are excluded. As the number of selected features increases, more discriminative features will be included, which will improve the clustering performance. When further increasing the features, noisy features rather than discriminative features will inevitably be included, thus degrading the clustering performance. In the case of different numbers of selected features, the clustering performance of some algorithms fluctuates significantly, but the NFRFS algorithm changes relatively smoothly, indicating that the number of selected features does not severely affect the clustering effect of NFRFS.

On the Yale, warpAR10P, ORL, JAFFE, TOX-171 and lung_small datasets, the clustering performance of NFRFS corresponding to all numbers of selected features is higher than that of other comparative algorithms. Briefly, regardless of the number of selected features, in most experimental results on all datasets, our proposed method is consistently superior to other state-of-the-art related methods.

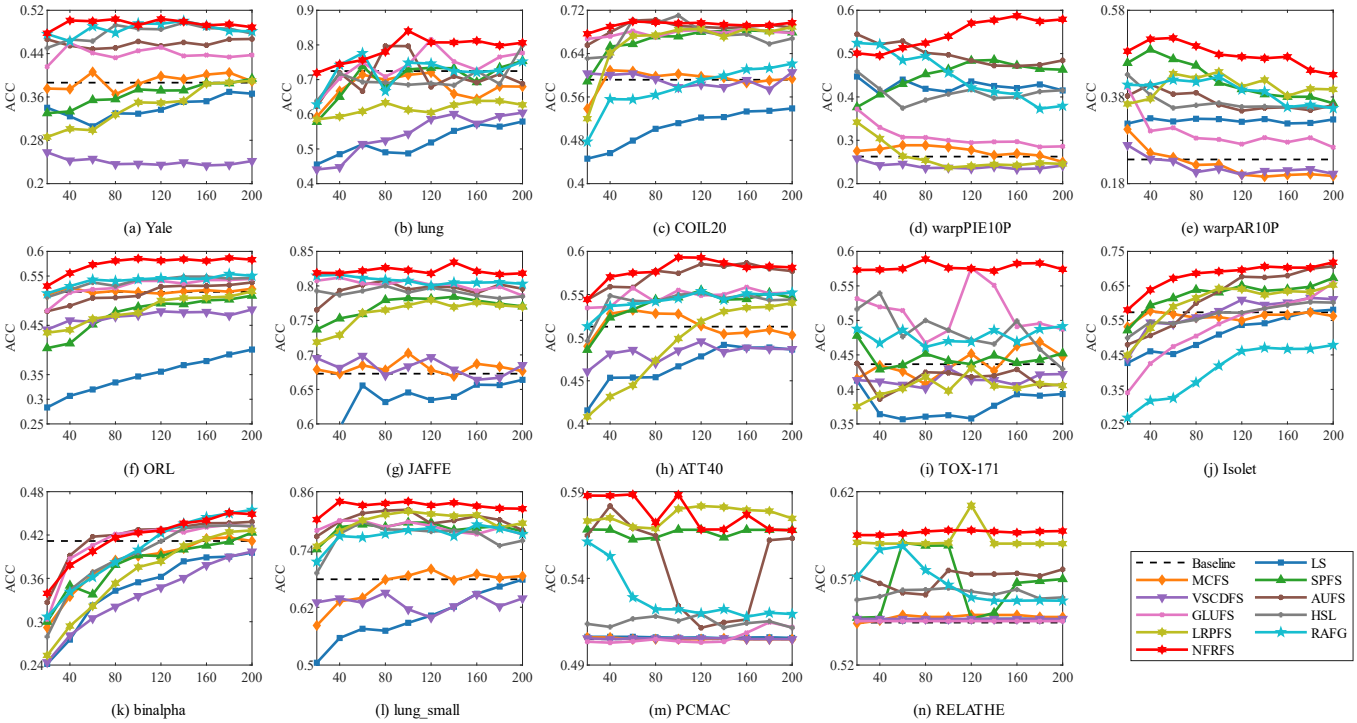


**Fig 2. ACC with different number of features on different datasets.**

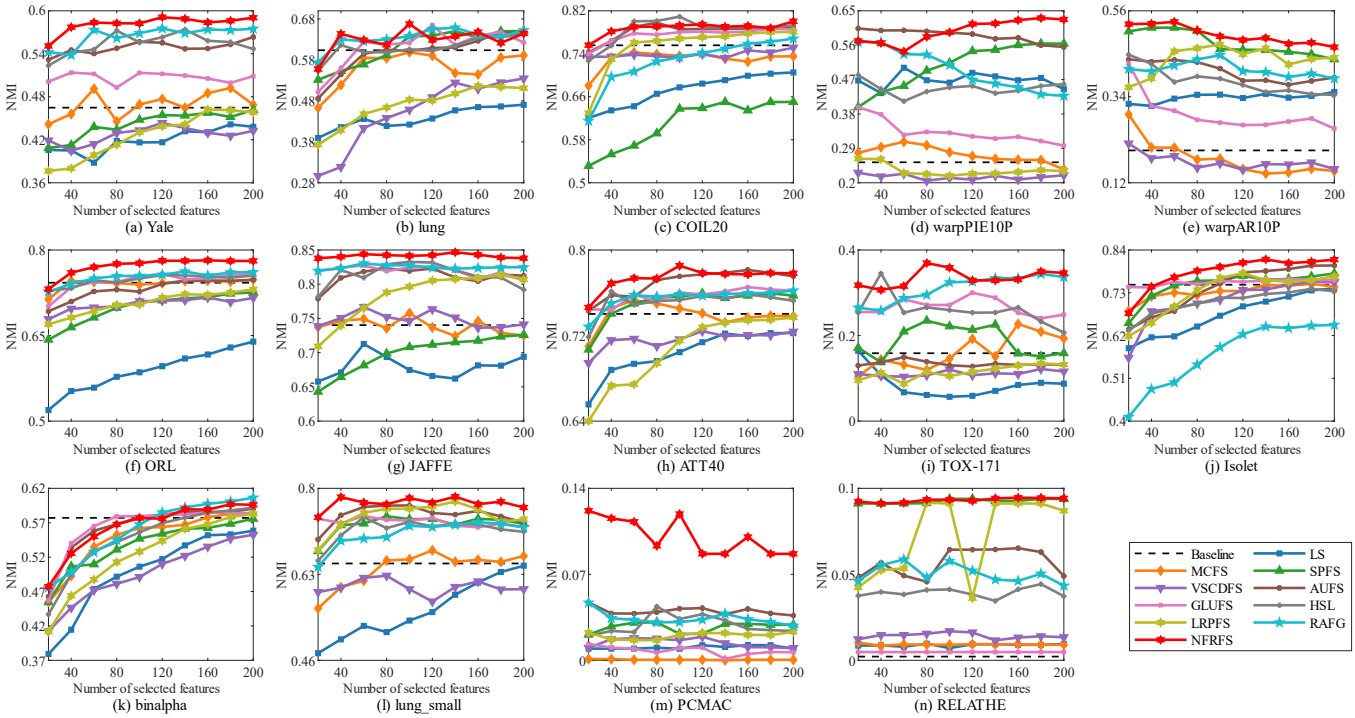


**Fig 3. NMI with different number of features on different datasets.**

## 4.6. Parameter sensitivity

To explore the impact of various parameters on how improving model performance, we choose 8 datasets to experiment a detailed analysis. There are three critical parameters $\alpha$ and $\beta$, and the $l_{2,p}$-norm parameter $p$ to innvolve the adjustment of in NFRFS algorithm. Specifically, $\alpha$ and $\beta$ are adjusted within range $\{10^{-6}, 10^{-4}, 10^{-2}, 1, 10^{2}, 10^{4}, 10^{6}\}$, while $p$ is tuned within range $p = \{0.01, 0.05, 0.1, 0.5, 1\}$. The parameter $\alpha$ controls the weight of manifold learning in the model, $\beta$ regulates the weight of the inner product regularization term in the feature selection matrix, and $p$ reflects the influence of adaptive distance metrics on the model. To isolate the effect of a single parameter, the other two parameters are fixed at 1 during the analysis.

Fig 4 and 5 display the influence of $\alpha$ on ACC and NMI across different datasets under varying numbers of selected features. The results indicate that when fewer features are selected, both ACC and NMI undergo significant changes. However, as the number of selected features increases, these metrics gradually stabilize. This is because a higher $\alpha$ enhances the weight of adaptive graph learning in the objective function, enabling the model to better exploit the intrinsic structure of the selected features and thus guide feature selection more effectively. For the PCMAC and RELATHE datasets, which have relatively low NMI values, changes in $\alpha$ lead to more pronounced impacts on clustering performance. Therefore, it is recommended that $\alpha$ be chosen from the range $\{1, 10^{2}, 10^{4}, 10^{6}\}$.

Fig 6 and 7 plot the effect of $\beta$ on ACC and NMI across different datasets and varying numbers of selected features. The results demonstrate that $\beta$ has a noticeable impact on small datasets, such as lung_small. However, in general, the clustering results

are more stable compared to variations in $\alpha$. This finding suggests that the inner product regularization of the feature selection matrix has a relatively minor effect on model performance.

Fig 8 and9 illustrate the impact of $p$ on ACC and NMI across different datasets and varying numbers of selected features. When $p = 1$, the JAFFE and binalpha datasets achieve the best clustering performance. However, for datasets like ATT40, lung_small, PCMAC, and RELATHE, clustering results are less favorable. This highlights that fixed distance metrics cannot universally adapt to the feature reconstruction spaces of all datasets. Thus, selecting an appropriate $p$ value based on the specific characteristics of each dataset is essential.

In conclusion, the optimal values of parameters $\alpha$, $\beta$, and $p$ differ across datasets to achieve the best average classification performance. Therefore, in practical applications, these parameters should be flexibly adjusted to obtain optimal results.

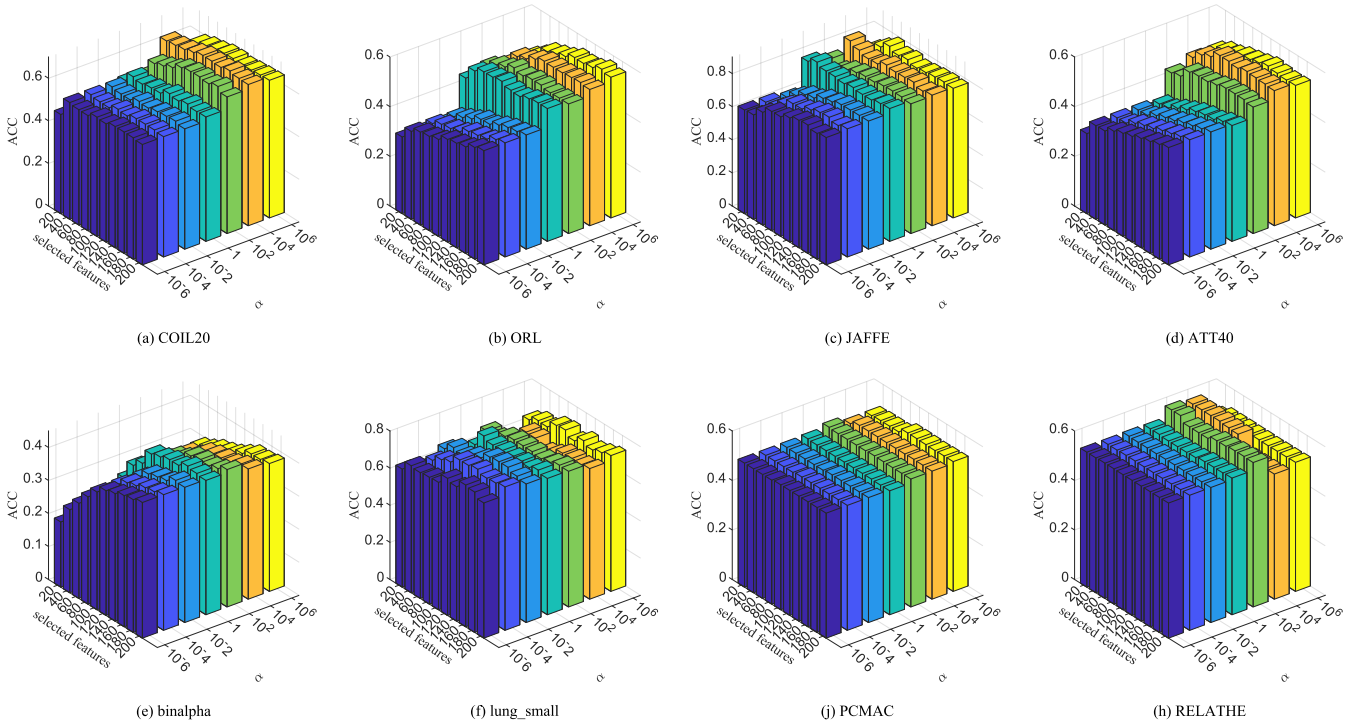


**Fig 4. ACC of NFRFS with different values of $\alpha$ on different datasets.**

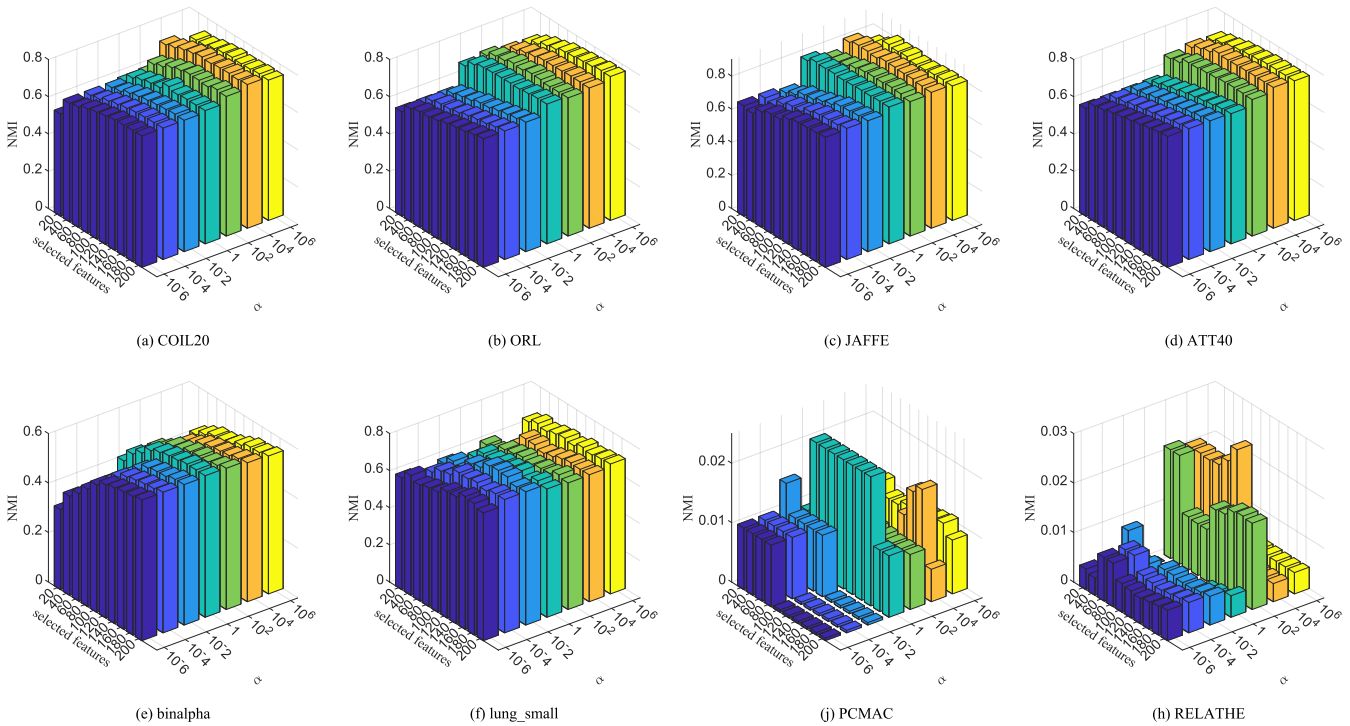


**Fig 5. NMI of NFRFS with different values of $\alpha$ on different datasets.**

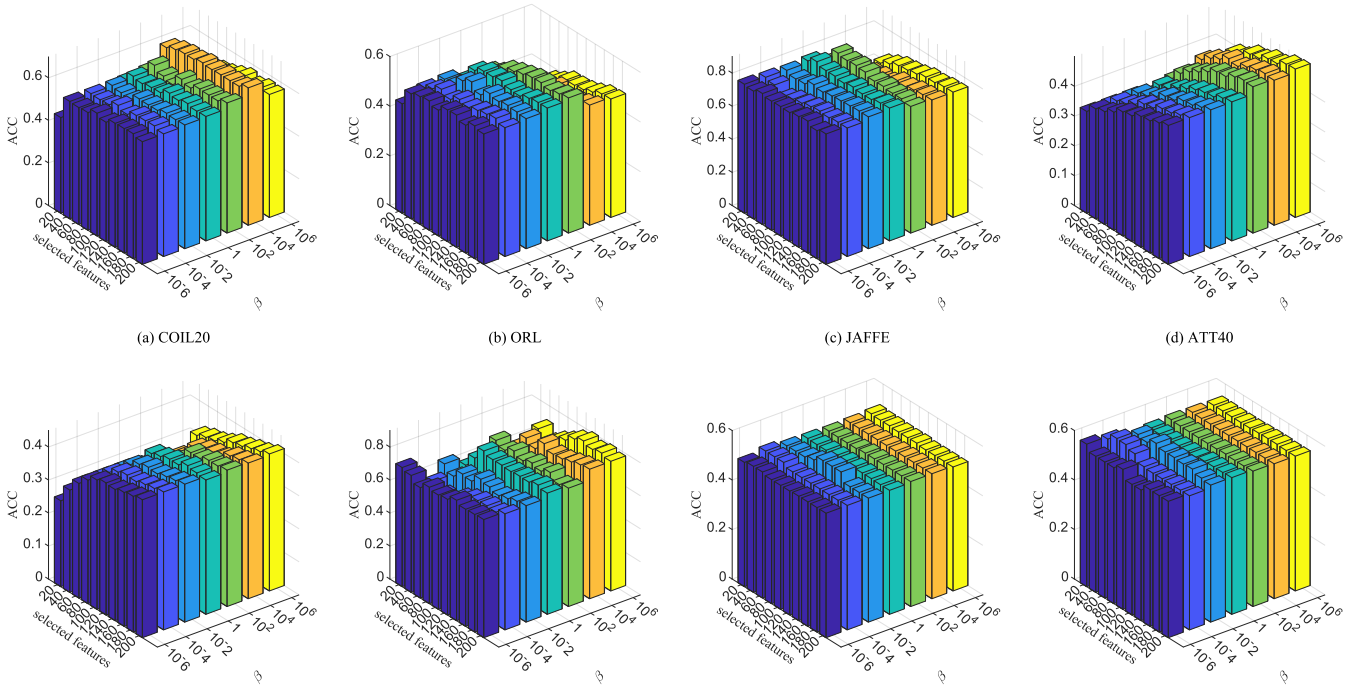


(a) COIL20 (b) ORL (c) JAFFE (d) ATT40

(e) binalpha (f) lung_small (j) PCMAC (h) RELATHE

**Fig 6. ACC of NFRFS with different values of $\beta$ on different datasets.**

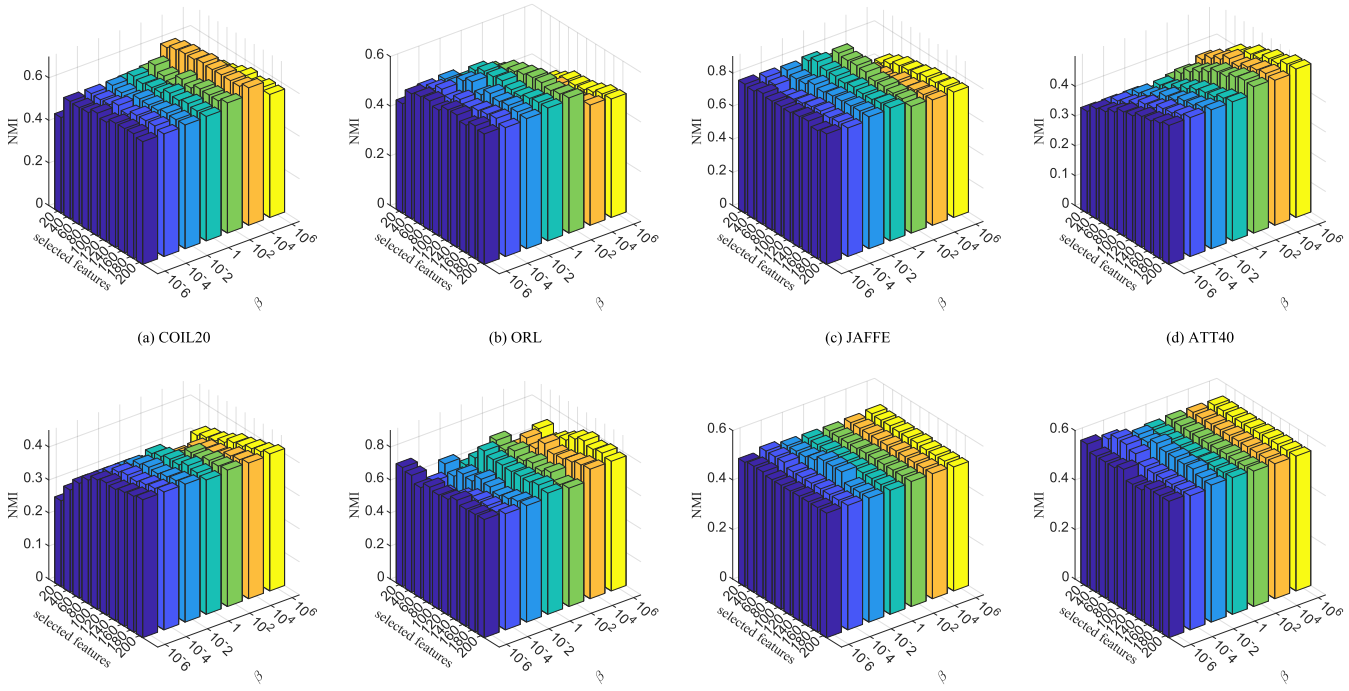


**Fig 7. NMI of NFRFS with different values of $\beta$ on different datasets.**

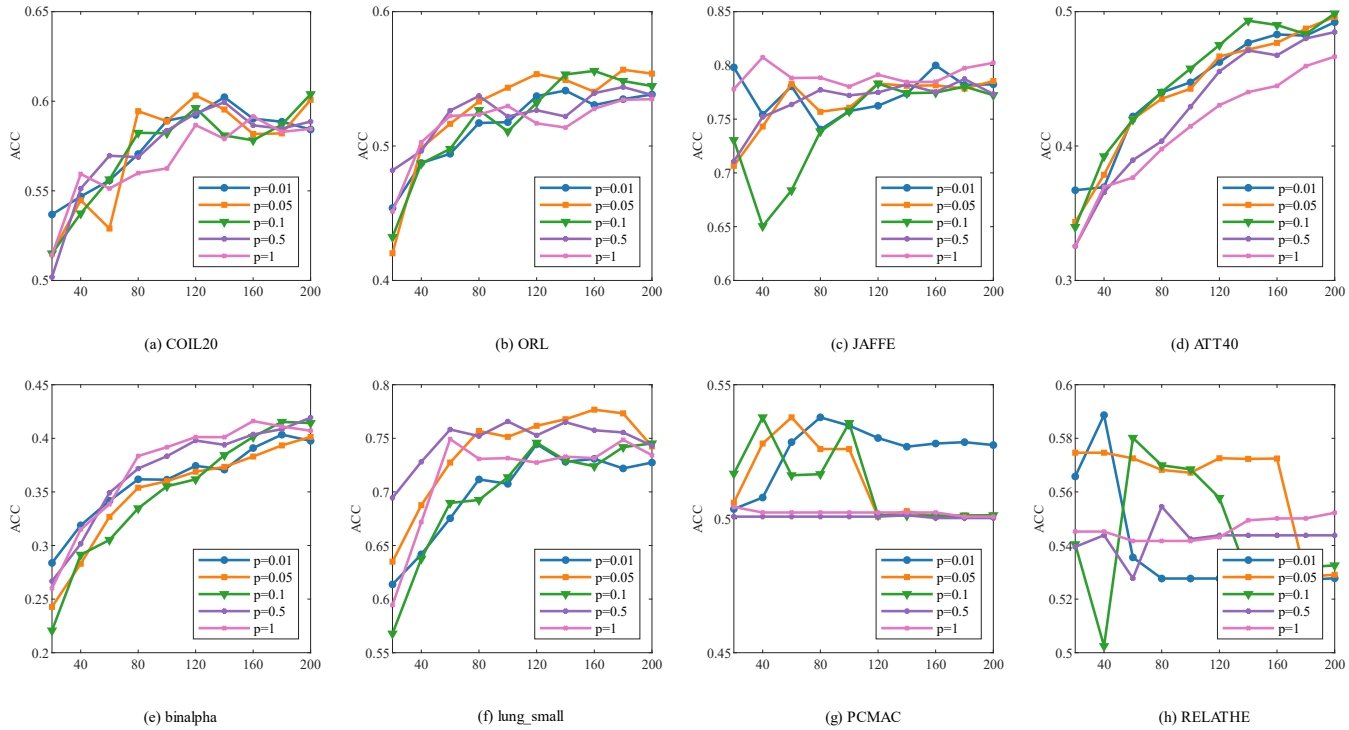


**Fig 8. ACC of NFRFS with different values of $p$ on different datasets.**

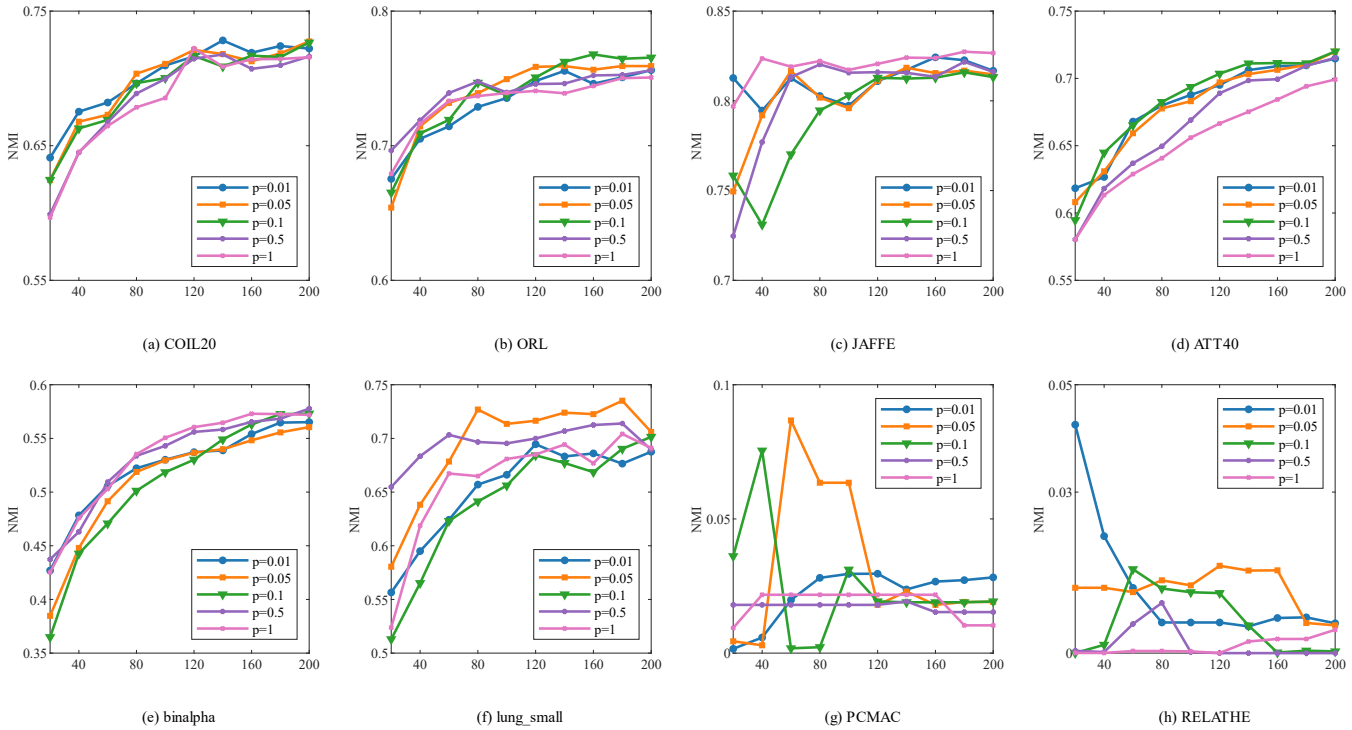


**Fig 9. NMI of NFRFS with different values of $p$ on different datasets.**

## 4.7. Robustness Evaluation

To evaluate the robustness of NFPFS, we compared the clustering results of GLUFS, HSL, LRPFS, and RAFG on the ORL face dataset. This dataset contains 400 face images of size 32×32 from 40 different classes. For each class, we introduced block noise of varying sizes into randomly selected images. Fig 10 shows representative images with block noise. The images in the first row have 10×10 block noise, those in the second row have 12×12 block noise, and those in the third row have 14×14 block noise. The results are illustrated in table 6 and 7. Based on these results, the performance of NFRFS is significantly better than other methods. This phenomenon indicates that our method is effective and superior in dealing with randomly distributed noise values and outliers.

**Fig 10. Representative images of the ORL face dataset with noise block.**

**Table 6. ACC of five algorithms on the ORL dataset with block noise**

| block | 10x10 | 12x12 | 14x14 |
|---|---|---|---|
| GLUFS | 40.06 | 36.79 | 34.71 |
| HSL | 49.64 | 49.42 | 46.06 |
| LPRFS | 39.47 | 38.86 | 37.72 |
| RAFG | 44.44 | 47.39 | 49.02 |
| NFRFS | 53.49 | 52.34 | 47.61 |

**Table 7. NMI of five algorithms on the ORL dataset with block noise.**

| block | 10x10 | 12x12 | 14x14 |
|---|---|---|---|
| GLUFS | 61.81 | 58.83 | 57.53 |
| HSL | 71.85 | 70.55 | 68.85 |
| LPRFS | 63.39 | 63.41 | 62.18 |
| RAFG | 69.06 | 69.63 | 68.62 |
| NFRFS | 75.22 | 74.17 | 69.72 |

## 4.8. Ablation study

This section will validate whether adaptive graph learning can enhance the model's clustering performance through ablation experiments. By setting the parameters, the following three effective combinations are obtained:

1. Baseline ($b$): the basic self-expression module which contains only the first and third items of eq (7),

$$\min ||X - XWH||_{2,p}^{p} + \beta(Tr(1_{d\times d}WW^{T}) - Tr(WW^{T})) \tag{39}$$

2.$b + \alpha + \beta$: the objective function of the baseline and the $\alpha$ weighted item,

$$\min ||X - XWH||_{2,p}^{p} + \alpha Tr(W^{T}X^{T}LXW) + \beta(Tr(1_{d\times d}WW^{T}) - Tr(WW^{T}))\min ||X - XWH$$

3. NFRFS: in our proposed method(NFRFS), the objective function of eq (7)

The clustering results Table 8 show the three combinations on our selected datasets warpPIE10P and JAFFE under the above three combinations. By comparing the feature selection results before and after introducing adaptive graph learning, the

improvement in model performance brought by graph learning is demonstrated. The reason lies in the fact that adaptive graph learning continuously updates the similarity matrix during the feature selection process, focusing on features with strong local correlations while preserving the global structure of the data. This dynamic interaction makes the feature selection process more robust and effective.

**Table 8. ACC and NMI of the component modules in our model.**

| | | Baseline (b) | $b+\alpha+\beta$ | NFRFS |
|---|---|---|---|---|
| **warpPIE10P** | ACC | 34.71 | 52.55 | 58.74 |
| | NMI | 57.53 | 62.17 | 63.10 |
| **JAFFE** | ACC | 80.19 | 79.79 | 83.43 |
| | NMI | 82.43 | 81.32 | 81.58 |

## 4.9. Convergence test

Additionally, the convergence results fig 11 speed of the method was studied through some numerical results. In fig 11, the horizontal axis represents the number of iterations, and the vertical axis represents the value of the objective function. The results indicate that with the objective function value decreasing very quickly and not increasing in subsequent iterations, which proposed method is effective and verifies the convergence.

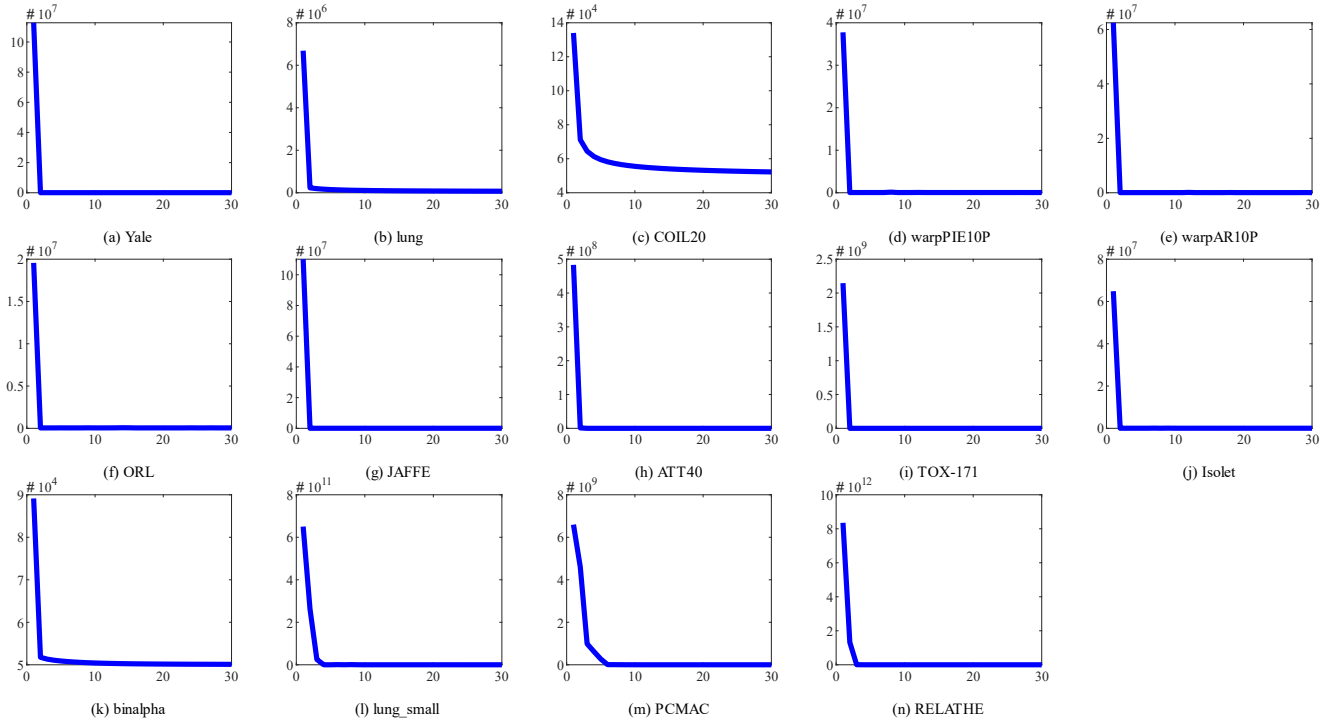


**Fig 11. Convergence curves of NFRFS on different datasets.**

## 5. Conclusion

In this study, we propose an unsupervised feature selection algorithm based on $l_{2,p}$-norm feature reconstruction, which employs the $l_{2,p}$-norm to flexibly adjust the distance between the original space and the reconstructed subspace, thereby enhancing the model's robustness to noise and outliers. By leveraging inner product sparse regularization, the rows and columns of the feature selection matrix are sparsified to select representative and low-redundancy features. Incorporating adaptive structure learning into the feature selection objective function helps preserve the local structure of the data. Experimental results demonstrate that the NFRFS algorithm exhibits excellent performance in feature selection across different datasets. However, determining the optimal hyperparameter $p$ in the feature reconstruction term in a more theoretical and efficient manner remains a direction for future research.

## References


1. Nießl C, Herrmann M, Wiedemann C, Casalicchio G, Boulesteix AL. Over-optimism in benchmark studies and the multiplicity of design and analysis options when interpreting their results. Wiley Interdisciplinary Reviews: Data Mining and Knowledge Discovery. 2022;12:e1441.

2. Saeys Y, Inza I, Larranaga P. A review of feature selection techniques in bioinformatics. bioinformatics. 2007;23:2507–2517.

3. Khalid S, Khalil T, Nasreen S. A survey of feature selection and feature extraction techniques in machine learning. In: 2014 science and information conference. IEEE; 2014. p. 372–378.

4. Reddy GT, Reddy MPK, Lakshmanna K, Kaluri R, Rajput DS, Srivastava G, et al. Analysis of dimensionality reduction techniques on big data. Ieee Access. 2020;8:54776–54788.

5. Huang H, Shi G, He H, Duan Y, Luo F. Dimensionality reduction of hyperspectral imagery based on spatial–spectral manifold learning. IEEE transactions on cybernetics. 2019;50:2604–2616.

6. Solorio-Fernández S, Carrasco-Ochoa JA, Martínez-Trinidad JF. A review of unsupervised feature selection methods. Artificial Intelligence Review. 2020;53:907–948.

7. Wang S, Tang J, Liu H. Embedded unsupervised feature selection. In: Proceedings of the AAAI conference on artificial intelligence. vol. 29; 2015.

8. Wang S, Zhu W. Sparse graph embedding unsupervised feature selection. IEEE Transactions on Systems, Man, and Cybernetics: Systems. 2016;48:329–341.

9. He X, Cai D, Niyogi P. Laplacian score for feature selection. Advances in neural information processing systems. 2005;18.

10. Tang C, Bian M, Liu X, Li M, Zhou H, Wang P, et al. Unsupervised feature selection via latent representation learning and manifold regularization. Neural Networks. 2019;117:163–178.

11. Du L, Shen YD. Unsupervised feature selection with adaptive structure learning. In: Proceedings of the 21th ACM SIGKDD international conference on knowledge discovery and data mining; 2015. p. 209–218.

12. Ma Z, Wei Y, Huang Y, Wang J. Unsupervised feature selection based on minimum-redundant subspace learning with self-weighted adaptive graph. Digital Signal Processing. 2024; p. 104738.

13. Emmert-Streib F, Dehmer M. High-dimensional LASSO-based computational regression models: regularization, shrinkage, and selection. Machine Learning and Knowledge Extraction. 2019;1:359–383.

14. Cai D, Zhang C, He X. Unsupervised feature selection for multi-cluster data. In: Proceedings of the 16th ACM SIGKDD international conference on Knowledge discovery and data mining; 2010. p. 333–342.

15. Nie F, Dong X, Tian L, Wang R, Li X. Unsupervised feature selection with constrained $l_{2,0}$-Norm and optimized graph. IEEE transactions on neural networks and learning systems. 2020;33:1702–1713.

16. Shang R, Liu C, Zhang W, Li Y, Xu S. Unsupervised feature selection method based on dual manifold learning and dual spatial latent representation. Expert Systems with Applications. 2024;255:124696.

17. Qi M, Wang T, Liu F, Zhang B, Wang J, Yi Y. Unsupervised feature selection by regularized matrix factorization. Neurocomputing. 2018;273:593–610.

18. Zhang M, Yang Y, Zhang H, Shen F, Zhang D. $l_{2,p}$-norm and sample constraint based feature selection and classification for AD diagnosis. Neurocomputing. 2016;195:104–111.

19. Wang S, Pedrycz W, Zhu Q, Zhu W. Subspace learning for unsupervised feature selection via matrix factorization. Pattern Recognition. 2015;48:10–19.

20. Shang R, Xu K, Shang F, Jiao L. Sparse and low-redundant subspace learning-based dual-graph regularized robust feature selection. Knowledge-Based Systems. 2020;187:104830.

21. Gong X, Yu L, Wang J, Zhang K, Bai X, Pal NR. Unsupervised feature selection via adaptive autoencoder with redundancy control. Neural Networks. 2022;150:87–101.

22. Saberi-Movahed F, Rostami M, Berahmand K, Karami S, Tiwari P, Oussalah M, et al. Dual regularized unsupervised feature selection based on matrix factorization and minimum redundancy with application in gene selection. Knowledge-Based Systems. 2022;256:109884.

23. Han J, Sun Z, Hao H. Selecting feature subset with sparsity and low redundancy for unsupervised learning. Knowledge-Based Systems. 2015;86:210–223.

24. Shang R, Xu K, Shang F, Jiao L. Sparse and low-redundant subspace learning-based dual-graph regularized robust feature selection. Knowledge-Based Systems. 2020;187:104830.

25. Qi M, Wang T, Liu F, Zhang B, Wang J, Yi Y. Unsupervised feature selection by regularized matrix factorization. Neurocomputing. 2018;273:593–610.

26. Zhang R, Zhang Y, Li X. Unsupervised feature selection via adaptive graph learning and constraint. IEEE Transactions on neural networks and learning systems. 2020;33:1355–1362.

27. Nie F, Zhu W, Li X. Unsupervised feature selection with structured graph optimization. In: Proceedings of the AAAI conference on artificial intelligence. vol. 30; 2016.

28. Huang P, Yang X. Unsupervised feature selection via adaptive graph and dependency score. Pattern Recognition. 2022;127:108622.

29. Bai H, Huang M, Zhong P. Precise feature selection via non-convex regularized graph embedding and self-representation for unsupervised learning. Knowledge-Based Systems. 2024;296:111900.

30. Sheikhpour R, Berahmand K, Mohammadi M, Khosravi H. Sparse feature selection using hypergraph Laplacian-based semi-supervised discriminant analysis. Pattern Recognition. 2025;157:110882.

31. Wang Z, Min W. Graph Regularized NMF with $l_{2,0}$-norm for Unsupervised Feature Learning. arXiv preprint arXiv:240310910. 2024;.

32. Li Z, Tang J. Unsupervised feature selection via nonnegative spectral analysis and redundancy control. IEEE Transactions on Image Processing. 2015;24(12):5343–5355.

33. Wang F, Zhu L, Li J, Chen H, Zhang H. Unsupervised soft-label feature selection. Knowledge-Based Systems. 2021;219:106847.

34. Wang S, Chen J, Guo W, Liu G. Structured learning for unsupervised feature selection with high-order matrix factorization. Expert Systems with Applications. 2020;140:112878.

35. Karami S, Saberi-Movahed F, Tiwari P, Marttinen P, Vahdati S. Unsupervised feature selection based on variance–covariance subspace distance. Neural Networks. 2023;166:188–203.

36. Cao Z, Xie X, Sun F. Adaptive unsupervised feature selection with robust graph regularization. International Journal of Machine Learning and Cybernetics. 2024;15:341–354.

37. Zhu P, Hou X, Tang K, Liu Y, Zhao YP, Wang Z. Unsupervised feature selection through combining graph learning and $l_{2,0}$-norm constraint. Information Sciences. 2023;622:68–82.

38. Mi Y, Chen H, Luo C, Horng SJ, Li T. Unsupervised feature selection with high-order similarity learning. Knowledge-Based Systems. 2024;285:111317.

39. Ma Z, Huang Y, Li H, Wang J. Unsupervised Feature Selection with Latent Relationship Penalty Term. Axioms. 2023;13(1):6.

40. Jiang K, Cao T, Zhu L, Sun Q. Adaptive and flexible $l_1$-norm graph embedding for unsupervised feature selection. Applied Intelligence. 2024;54(22):11732–11751.

41. Liu G, Guo Z, Liu W, Jiang F, Fu E. A feature selection method based on the Golden Jackal-Grey Wolf Hybrid Optimization Algorithm. Plos one. 2024;19(1):e0295579.

42. Tang C, Zheng X, Zhang W, Liu X, Zhu X, Zhu E. Unsupervised feature selection via multiple graph fusion and feature weight learning. Science China Information Sciences. 2023;66:152101.

# Supporting information

**S1 Data.**